Magnetic Field Generated by the Loops Used in Traffic Control Systems

Antonio Mocholí-Salcedo, José Humberto Arroyo-Núñez, Víctor M. Milián-Sánchez, María J. Palomo-Anaya, and Alexander Arroyo-Núñez

***Abstract*— In this paper, a detailed study about the value, in any point of space $P(x, y, z)$, of the magnetic field generated by a rectangular loop that carries a current I has been made. The analysis focuses on the study of rectangular magnetic loops that are used as sensors in traffic control systems. The inductance of magnetic loops is calculated numerically in three different ways, and the optimal way of performing the numerical summation is derived, which takes into account the magnetic field singularity on the conductor itself. The calculations also take into account the distance between the different turns in the loop. Later, the results are compared with the most commonly used empirical methods for inductance calculation. This paper shows the great similarity between empirical and numerically calculated results and concludes with the experimental verification and validation of the obtained theoretical results. Thus, both the system to evaluate the results and the proposed numerical methods for inductance calculation can be used in other loops geometries. This methodology can also be used for the mutual inductance calculation that appears between a buried loop and any kind of vehicle geometry, whose oscillation frequency variation determines the magnetic signature. The mutual inductance calculation can be used to determine the signal level that can be exchanged between the loops on the pavement and those on the vehicle, which in turn can be used as a short-range communication system between vehicles and infrastructures, with applications such as vehicles classification, speed measurements, or communication between vehicles.**

***Index Terms*— Inductance in rectangular coils, inductive communication, magnetic field, numerical calculation, vehicle detection.**

I. Introduction

IT HAS been many years since magnetic loops have been used as basic sensors for vehicles detection. The operating principle is very simple: when a metallic mass (the vehicle) passes over the loop connected to an oscillating circuit, the loop inductance is altered and consequently a change in the oscillating frequency takes place, which in turn is detected by the control system [1]. The obtained results are very reliable and therefore it is still considered as the reference detector system [2], [3].

Taking into account the success of this device and its widespread deployment in every road of the world, several authors have proposed other applications, like the classification of vehicles by means of their magnetic footprint [4], [5], the bi-directional communication between vehicles and infrastructures [6] or vehicles speed measurement [7]–[10]. Moreover, a variation of this system consisting in a quadrupole loop can be used to improve detection of bicycles [11].

These applications require a precise knowledge about the magnetic field generated by the rectangular magnetic loops. Most of the textbooks analyze circular loops, whose symmetry allows a great simplification of the calculations [12]. In other cases where rectangular loops have been analyzed, simplifications arise because the magnetic field is studied at very short or very large distances relatively to the loops dimensions; this allows to perform considerable simplifications in the calculations [13].

However, in the case of the loops used in the traffic control systems the studied phenomena take place at a distance of the same order of magnitude than the loop size. Therefore in the corresponding analysis it is not possible to perform any simplification in the calculation of the magnetic fields. But the current computing tools allow us to perform such analysis.

Specifically, this work analyses in detail the magnetic field in any point of space, P(x,y,z), generated by a rectangular loop that carries a current I. The expressions to obtain the magnetic field generated by rectangular loops are analyzed and later, different methods to obtain those loops inductance in an optimized way are proposed. The results obtained by means of numerical methods are compared with those obtained with both the application of formulae proposed by other authors and the experimental measurements.

II. Theoretical Analysis of the Magnetic Field Generated by a Rectangular Loop

The following analysis starts with the application of Maxwell equations. According to them, the divergence of the magnetic field ($\vec{B}$) equals zero [12],

$$\vec{\nabla} \cdot \vec{B} = 0 \tag{1}$$

To enable the simplification of calculations, $\vec{B}$ can be represented using the auxiliary vectorial function $\vec{A}$ in such

Manuscript received November 23, 2015; revised February 10, 2016 and July 31, 2016; accepted November 17, 2016. This work was supported in part by the Ministry of Education of Spain and in part the company ETRA I+D S.A. The Associate Editor for this paper was B. F. Ciuffo.

A. Mocholí-Salcedo is with the Traffic Control Systems Group, ITACA, Universitat Politècnica de València, 46022 Valencia, Spain (e-mail: amocholi@eln.upv.es).

J. H. Arroyo-Nuñez is with the Electronic and Telecommunications Engineering Department, Polytechnic University of Tulancingo, Tulancingo 43600, Mexico (e-mail: humberto.arroyo@upt.edu.mx).

V. M. Milián-Sánchez is with the Institute for Industrial, Radiological and Environmental Safety, Universitat Politècnica de València, 46022 Valencia, Spain (e-mail: vicmisan@iqn.upv.es).

M. J. Palomo-Anaya is with the Chemical and Nuclear Engineering Department, Universitat Politècnica de València, 46022 Valencia, Spain (e-mail: mpalomo@iqn.upv.es).

A. Arroyo-Nuñez is with the Biomedical Engineering Department, Polytechnic University of Chiapas, Suchiapa 29150, Mexico (e-mail: arroyo@upchiapas.edu.mx).

Digital Object Identifier 10.1109/TITS.2016.2632972

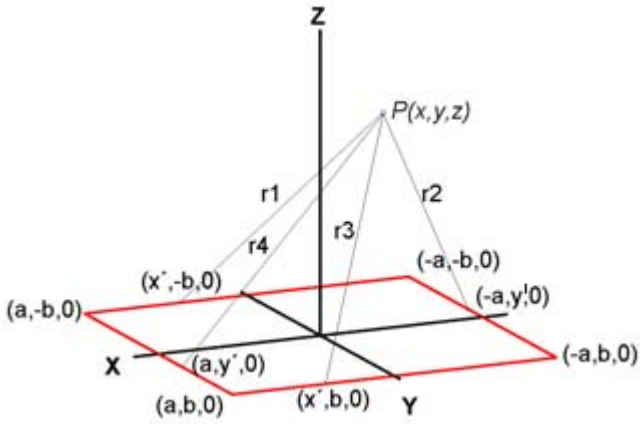

Fig. 1. Magnetic loop and point P(x,y,z) where the analysis of the magnetic field is performed.

a way that:

$$\vec{\mathrm{B}} = \vec{\nabla}\,\mathrm{x}\,\vec{\mathrm{A}} \tag{2}$$

That is, $\vec{\mathrm{B}}$ is the rotational of $\vec{\mathrm{A}}$. Substituting (2) in (1) one obtains:

$$\vec{\nabla}\cdot\left(\vec{\nabla}\mathrm{x}\vec{\mathrm{A}}\right) = 0 \tag{3}$$

$\vec{\mathrm{A}}$ is the *magnetic vector potential field*. This field is related to the current density, $\vec{\mathrm{J}}$, which in turn originates $\vec{\mathrm{B}}$. In the case of a current along a linear conductor, $\vec{\mathrm{A}}$ is defined by:

$$\vec{\mathrm{A}} = \int_l \frac{\mu_o \vec{\mathrm{I}} \mathrm{d}l'}{4\pi\,\mathrm{r}} \tag{4}$$

where:

$\vec{\mathrm{I}}$ is the current in the linear conductor,
r is the distance from each point of the conductor to the point where the field is analyzed.

The solution represented by (4) has been obtained on the basis of the only two assumptions that have been made in our study: a) conductors are thin (i.e., the diameter is much lower than the distance at which the field is studied) and b) the loop carries a stationary current. However, the general solution would include the conductor volumetric integral [12].

In order to analyze a thin wire rectangular loop, the magnetic field is calculated as the sum of all contributions to the field generated by each section of the loop. In Fig. 1, a magnetic loop centered in the XY plane is shown, as well as the point P(x,y,z) where the field is analyzed.

Here, r1, r2, r3, and r4 represent the distances between each point of the sections that form the loop and the point where the magnetic field is analyzed. These distances are obtained from the following expressions:

$$\begin{aligned} r1 &= \sqrt{(x-x')^2+(y+b)^2+z^2} \\ r2 &= \sqrt{(x+a)^2+(y-y')^2+z^2} \\ r3 &= \sqrt{(x-x')^2+(y-b)^2+z^2} \\ r4 &= \sqrt{(x-a)^2+(y-y')^2+z^2} \end{aligned} \tag{5}$$

The magnetic field in P(x,y,z) is calculated by means of vector $\vec{\mathrm{A}}$, given in (4). This calculation is performed assuming a clockwise current "I" in the loop.

Given that the low frequencies are the ones of interest in the applications of traffic control systems, one can assume a stationary current in the loop, i.e., the current intensity is the same in every point of the loop. This makes this study applicable in the case of low frequency variable currents (generally below 1 MHz).

The magnetic vector potential corresponding to the loop section located between (a,−b,0) and (−a,−b,0) is defined by $\vec{A}_{1x}$. Substituting r1 of (5) in (4) one obtains:

$$\vec{A}_{1x} = \frac{\mu_0 I}{4\pi}\int_a^{-a} \frac{dx'}{\sqrt{(x-x')^2+(y+b)^2+z^2}}$$

This integration yields [14]:

$$\vec{A}_{1x} = \frac{\mu_0 I}{4\pi}\ln\frac{\sqrt{(x+a)^2+(y+b)^2+z^2}-a-x}{\sqrt{(x-a)^2+(y+b)^2+z^2}+a-x} \tag{6}$$

The magnetic vector potential which corresponds to the loop section located between (−a,−b,0) and (−a,b,0) is defined by $\vec{A}_{2y}$. Similarly the previous calculation of $\mathrm{A_{1x}}$, when using the distance r2 this component reads:

$$\vec{A}_{2y} = \frac{\mu_0 I}{4\pi}\ln\frac{\sqrt{(x+a)^2+(y-b)^2+z^2}+b-y}{\sqrt{(x+a)^2+(y+b)^2+z^2}-b-y} \tag{7}$$

For the loop section located between (−a,b,0) y (a,b,0) the magnetic vector potential is defined as $\vec{A}_{3x}$. Thus, using r3 one obtains:

$$\vec{A}_{3x} = \frac{\mu_0 I}{4\pi}\ln\frac{\sqrt{(x-a)^2+(y-b)^2+z^2}+a-x}{\sqrt{(x+a)^2+(y-b)^2+z^2}-a-x} \tag{8}$$

The loop section located between (a,b,0) y (a,-b,0) has a magnetic vector potential defined as $\vec{A}_{4y}$; using r4 this component can be written as:

$$\vec{A}_{4y} = \frac{\mu_0 I}{4\pi}\ln\frac{\sqrt{(x-a)^2+(y+b)^2+z^2}-b-y}{\sqrt{(x-a)^2+(y-b)^2+z^2}+b-y} \tag{9}$$

With the purpose of simplifying the representation of vector $\vec{\mathrm{A}}$ one can define:

$$\begin{aligned} R1 &= \sqrt{(x+a)^2+(y+b)^2+z^2} \\ R2 &= \sqrt{(x-a)^2+(y+b)^2+z^2} \\ R3 &= \sqrt{(x+a)^2+(y-b)^2+z^2} \\ R4 &= \sqrt{(x-a)^2+(y-b)^2+z^2} \\ c1 &= -a-x \\ c2 &= a-x \\ d1 &= -b-y \\ d2 &= b-y \end{aligned} \tag{10}$$

Substituting the values of (10) in (6), (7), (8), and (9):

$$\begin{aligned}\vec{A}_{1x} &= \frac{\mu_0 I}{4\pi}\ln\frac{R1+c1}{R2+c2}\\ \vec{A}_{2y} &= \frac{\mu_0 I}{4\pi}\ln\frac{\mathrm{R3+d2}}{\mathrm{R1+d1}}\\ \vec{A}_{3x} &= \frac{\mu_0 I}{4\pi}\ln\frac{\mathrm{R4+c2}}{\mathrm{R3+c1}}\\ \vec{A}_{4y} &= \frac{\mu_0 I}{4\pi}ln\frac{R2+d1}{R4+d2}\end{aligned} \tag{11}$$

Adding components "x" and "y" we obtain:

$$\begin{aligned}\vec{A}_x &= \frac{\mu_0 I}{4\pi}\ln\left[\frac{R1+c1}{R2+c2} * \frac{\mathrm{R4+c2}}{\mathrm{R3+c1}}\right]\\ \vec{A}_y &= \frac{\mu_0 I}{4\pi}\ln\left[\frac{\mathrm{R3+d2}}{\mathrm{R1+d1}} * \frac{\mathrm{R2+d1}}{\mathrm{R4+d2}}\right]\end{aligned} \tag{12}$$

The magnetic vector potential $\vec{A}$ has only "x" and "y" components because from (4) one can see that $\vec{A}$ is a line integral along the loop, and since the loop has no Z component, $\vec{A}$ will not have it either.

From $\vec{A}$ it is possible to calculate the magnetic field by means of (2). Then,

$$\vec{B} = \left(-\frac{d}{dz}A_y\right)\vec{i} + \left(\frac{d}{dz}A_x\right)\vec{j} + \left(\frac{d}{dx}A_y - \frac{d}{dy}A_x\right)\vec{k} \tag{13}$$

Equation (13) is the magnetic field in point P(x,y,z), which has three components; its analysis requires the calculation of each one of them.

For component "x" one obtains:

$$\begin{aligned}\vec{B}_i = \frac{\mu_0 I}{4\pi}\Bigg[&\frac{z}{R1(R1+d1)} - \frac{z}{R2(R2+d1)}\\ &- \frac{z}{R3(R3+d2)} + \frac{z}{R4(R4+d2)}\Bigg]\end{aligned} \tag{14}$$

Component "y" is given by:

$$\begin{aligned}\vec{B}_j = \frac{\mu_0 I}{4\pi}\Bigg[&\frac{z}{R1(R1+c1)} - \frac{z}{R2(R2+c2)}\\ &- \frac{z}{R3(R3+c1)} + \frac{z}{R4(R4+c2)}\Bigg]\end{aligned} \tag{15}$$

And component "z" is given by:

$$\begin{aligned}\vec{B}_k = \frac{\mu_0 I}{4\pi}\Bigg(\Bigg[&-\frac{(x+a)}{R1(R1+d1)} + \frac{(x-a)}{R2(R2+d1)}\\ &+ \frac{(x+a)}{R3(R3+d2)} - \frac{(x-a)}{R4(R4+d2)}\Bigg]\\ &-\Bigg[\frac{(y+b)}{R1(R1+c1)} - \frac{(y+b)}{R2(R2+c2)}\\ &- \frac{(y-b)}{R3(R3+c1)} + \frac{(y-b)}{R4(R4+c2)}\Bigg]\Bigg)\end{aligned} \tag{16}$$

Since (14), (15), and (16) are the magnetic field components in point P(x,y,z), its module is:

$$\left|\vec{B}\right| = \sqrt{(B_i)^2 + \left(B_j\right)^2 + (B_k)^2} \tag{17}$$

These Equations have been checked against those presented by Misakian [13], where one can see the expressions of a magnetic field produced by one or more rectangular loops located in the same plane.

III. Results of Theoretical Analysis

From the expressions obtained in previous theoretical analysis, it is possible to represent, in any point of space, the module of the magnetic field generated by a rectangular loop.

In what follows, one can see a set of representations of the magnetic field generated by a rectangular loop of dimensions 2x1 m at different heights from the loop that carries a current of 100 mA.

In Fig. 2a, a scheme of the analyzed rectangular loop is presented.

Fig. 2b represents the module of the magnetic field strength generated by the loop on a parallel plane of 4x4 m dimensions and at a height of 50 cm. The graph was obtained point by point from (17). A surface slightly bigger than that of the loop (with the aim of observing the range of the magnetic field beyond the contour of the loop) has been chosen.

In both Fig. 2c and Fig. 2d the magnetic field at 25 cm and 5 cm height respectively is represented.

A. Loop Parameters Derivation

Once the magnetic field generated by the loop in each point of space has been obtained, the next step consists in deriving the loop's electrical parameters such as the resistance and inductance.

The equivalent series loop resistance R_L can be obtained from both conductor's ohmic resistance R (which includes the frequency contribution) and ground resistance R_g and is:

$$R_L = R + R_g \tag{18}$$

The loop ohmic resistance R depends on the operating frequency; at low frequency it can be obtained from the cables length, conductor radius, its resistivity and the number of turns and is:

$$R_{i0} = \rho\frac{l}{S} = \rho\frac{2(2a+2b)N}{\pi R_C^2} \tag{19}$$

where

- R_{i0} : loop's ohmic resistance at low frequency (ohm)
- ρ : conductor resistivity (ohm·m)
- R_c : conductor radius (m)
- N : number of turns

But the resistance formula which includes the effect of the high frequency is given by Johnson [15] and is:

$$R = R_{i0}\frac{q}{2}\left[\frac{ber\,(q)\times bei^{'}\,(q) - bei\,(q)\times ber^{'}(q)}{\left(bei^{'}(q)\right)^2 + \left(ber^{'}(q)\right)^2}\right] \tag{20}$$

In (20), $ber\,(q)$ is the real part of the complex Bessel function of first kind, $ber'\,(q)$ is the first derivative of the complex Bessel function of first kind, $bei\,(q)$ is the imaginary part of the complex Bessel function of first kind, $bei'\,(q)$ is the first derivative of the imaginary part of the complex Bessel function of first kind, where:

$$q = \frac{R_C\sqrt{2}}{\delta} \tag{21}$$

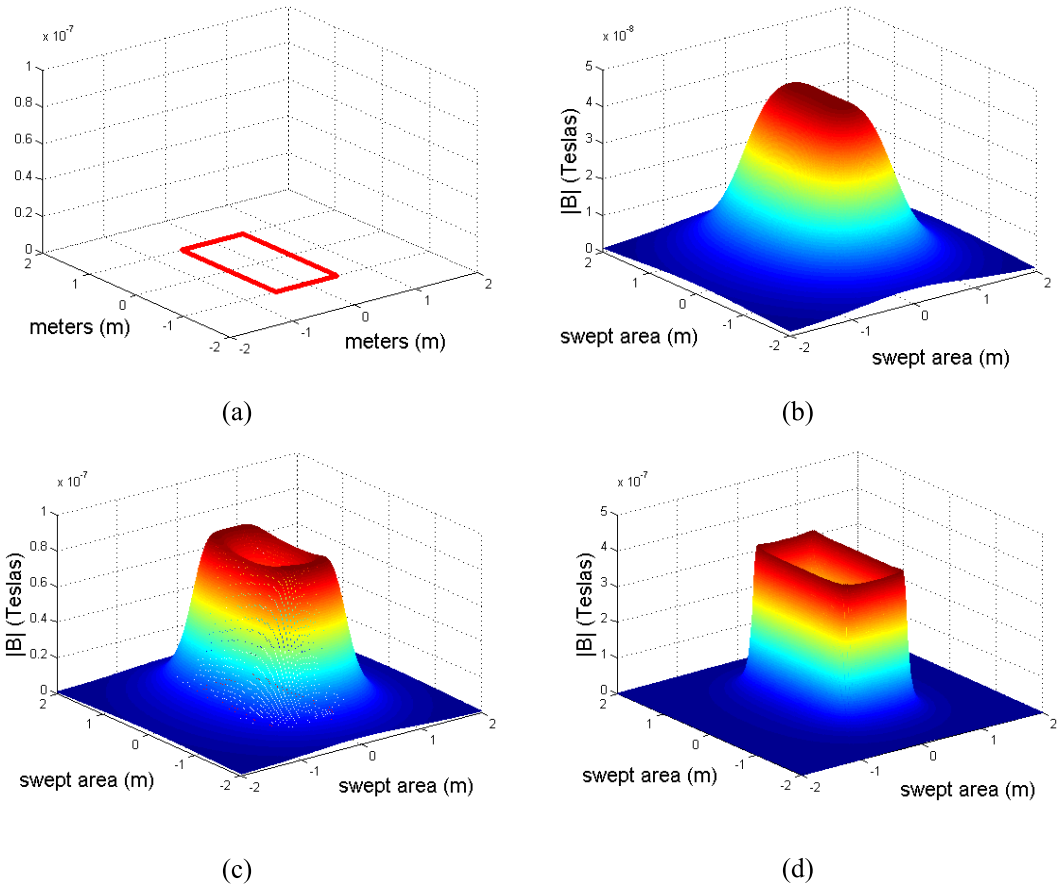

Fig. 2. a) Loop of dimensions 2x1 m on the XY plane. b) Magnetic field module at 50 cm above the plane of the loop. c) Magnetic field module at 25 cm above the plane of the loop. d) Magnetic field module at 5 cm above the plane of the loop.

and:

$$\delta = \frac{1}{\sqrt{\mu_r \mu_0 \pi f \sigma}} \tag{22}$$

where:

μ_0 = air or free space permeability $= 4\pi \cdot 10^{-7}$ H/m
μ_r = copper wire relative permeability $= 1$
f = operation frequency (Hz)
σ = copper wire conductivity $= 0.58 \cdot 10^8$ mhos/m

Ground resistance R_g is caused by the current induced in the conducting substances existing in the pavement and subgrade material surrounding the loop. This resistance can reduce detector's sensibility in those pavement locations where a high quantity of conductors exists, as well as in locations with high humidity content. Its calculation is performed assuming that pavement magnetic losses are similar to those originated by a ferrite or iron core in a coil. It is also assumed that relative permeability $\mu_g = 1$. Under these conditions ground resistance is given by [16]:

$$R_g = \omega L_L \tan \delta_g \tag{23}$$

where:

$\tan \delta_g$ = loss tangent of pavement material (a typical value is about 0.01)
L_L = coil self-inductance (H)
ω = angular frequency $= 2\pi f$ (radians s^{-1})
f = operating frequency (Hz)

Regarding the inductance, its calculation can be performed by means of:

$$L_\emptyset = \frac{N\emptyset}{I} \tag{24}$$

where:

$L_\emptyset$: loop inductance
$\emptyset$: magnetic flux crossing and generated by the loop
I : current in the loop
N : turns in the loop

The magnetic flux crossing the loop is calculated (numerically) by the surface integral of the product of the normal component of the magnetic field passing through the loop surface:

$$\emptyset = \int_S \vec{B} \cdot \overrightarrow{dS} \tag{25}$$

In this case the loop is rectangular; it is placed on the XY plane and centered in the origin of coordinates. The lengths of their sides are 2a and 2b, and they are parallel to x and y axis. Under these conditions we are only interested in the normal component of the magnetic field, B_k, because the surface vector only has one component parallel to Z axis. The infinitesimal surface element dS can be considered as the product of the two elements of longitude dydx according to the Y and X axis. Taking all this in account,

one can write:

$$\emptyset = \int_S \vec{B} \cdot \vec{d}S = \int_{-a}^{a} \int_{-b}^{b} B_K \, dy \, dx \tag{26}$$

This integration can be solved numerically substituting the integrals by summations. To this end, it is necessary to obtain the magnetic field value in a succession of points in space limited by a surface element $dydx$. If Nx and Ny are the number of points (along X and Y axis respectively) where the magnetic field is going to be measured, we obtain for the elementary lengths:

$$\begin{aligned} dx &= \frac{2a}{N_x} \\ dy &= \frac{2b}{N_y} \end{aligned} \tag{27}$$

In (26) B_k can be expressed as $B_K(x, y, z)$, which is the magnetic field component parallel to Z axis in point (x,y,z). Thus the flux through the loop surface can be given by:

$$\emptyset = \sum_{n=1}^{N_x - 1} \sum_{m=1}^{N_y - 1} B_K(-a + ndx, -b + mdy, 0) \, f_x \, f_y \, dy \, dx \tag{28}$$

The summation limits have been chosen with the purpose of avoiding the magnetic field measurement on the conductors themselves because of the singularity that B_K presents on those points. In this way, summations are delimited by $(-a + dx, a - dx)$ and $(-b + dy, b - dy)$ on X and Y axis respectively. But this procedure causes a measurement error which has been reduced by increasing the surface element in 50% at the summation intervals located nearby the boundaries. For this purpose, one can use the factors f_x and f_y in such a way that $f_x = 1$ in every point except in $n = 1$ and $n = N_x - 1$, where $f_x = 1.5$. Similarly, $f_y = 1$ in every point except in $m = 1$ and $m = N_y - 1$, where $f_y = 1.5$. By means of these two factors, it is possible to avoid taking measurements just on the conductors; their values were selected by trial and error.

Due to the abrupt change that appears in magnetic field component B_K located in the proximity of the conductors, it is necessary to make a proper election of N_x and N_y. The following paragraphs explain how this can be achieved.

Firstly, to compute the inductance of a rectangular loop, we used one of the most common approximated expressions given by Grover [17]:

$$\begin{aligned} L_G = \frac{N^2 \mu}{\pi} & \left(-2\,(2a + 2b) + 2\sqrt{(2a)^2 + (2b)^2} \right. \\ & -2a \; ln\left(\frac{2a + \sqrt{(2a)^2 + (2b)^2}}{2b} \right) \\ & -2b \; ln\left(\frac{2b + \sqrt{(2a)^2 + (2b)^2}}{2a} \right) \\ & \left. +2a \log \frac{2a}{R_C} + 2b \log \frac{2b}{R_C} \right) \end{aligned} \tag{29}$$

Secondly, to determine the number of integration points N_p to be taken in (28), the results obtained using both (24) and (29) were compared. To do this, inductances were calculated for different rectangular loops dimensions, different number of turns and different number of points in the numeric integral. The results comparison obtained by means of these calculations are shown in Fig. 3. In this Figure one can see the difference in results (relative error, E_r) obtained with both the numeric integral and the approximated formula for different loop dimensions and for different conductor radius R_c, where the relative error is given by:

$$E_r = \frac{L_\emptyset - L_G}{L_G} \cdot 100\,(\%)\,,$$

where L_G is taken as the reference value. Also, each Figure corresponds to different number of integration points, N_p.

The analysis of the relative errors (considered in absolute value), shown in these Figures reveals that:

- For every specific loop dimensions and cable diameter, error is independent from the number of turns (in the example of Fig. 3a, the case for Rc = 0.0002 m is represented).
- For every loop dimensions and cable diameter, error depends on the number of points that have been used for numeric integration.
- The minimal error is achieved when the integration is performed for a number of points given by (30) (Fig. 3d):

$$N_x = \frac{2a}{3R_C}; \; N_y = \frac{2b}{3R_C} \tag{30}$$

Taking these numbers of integration points, the obtained relative error is less than 0.5%; the only limitation is that they must be higher than 20. But even for a low number of points relative error is less than 1%.

- If the number of points increases above the values given by (30), as in Fig. 3b and 3c, the inductance obtained by means of the integration technique, Lϕ, is progressively higher than the one obtained with the approximated Equation, (29).
- If the number of points decreases below the values given by (30), as in Fig. 3e and 3f, the inductance obtained by means of the integration technique is progressively lower than the one obtained with the approximated Equation.
- As the ratio between the loop dimensions and the cable diameter diminishes, it is apparent that the difference between the inductance obtained with the integration technique and the approximated formula increases; likewise, for a given loop dimensions, relative error increases with higher wire diameter.
- This difference also increases when the loop dimensions diminish. In other words, for a given Rc value, relative error increases (in module) when the loop dimensions diminish.

It must be highlighted that the trends of the relative error for the different graphs in Fig. 3d differ from the trends in previous and posterior subfigures of Fig. 3. This is due to the relative errors being below 1% and therefore, the rounding errors can be of the same order of magnitude as the calculation errors. This leads to relative error oscillations, with values very close to zero.

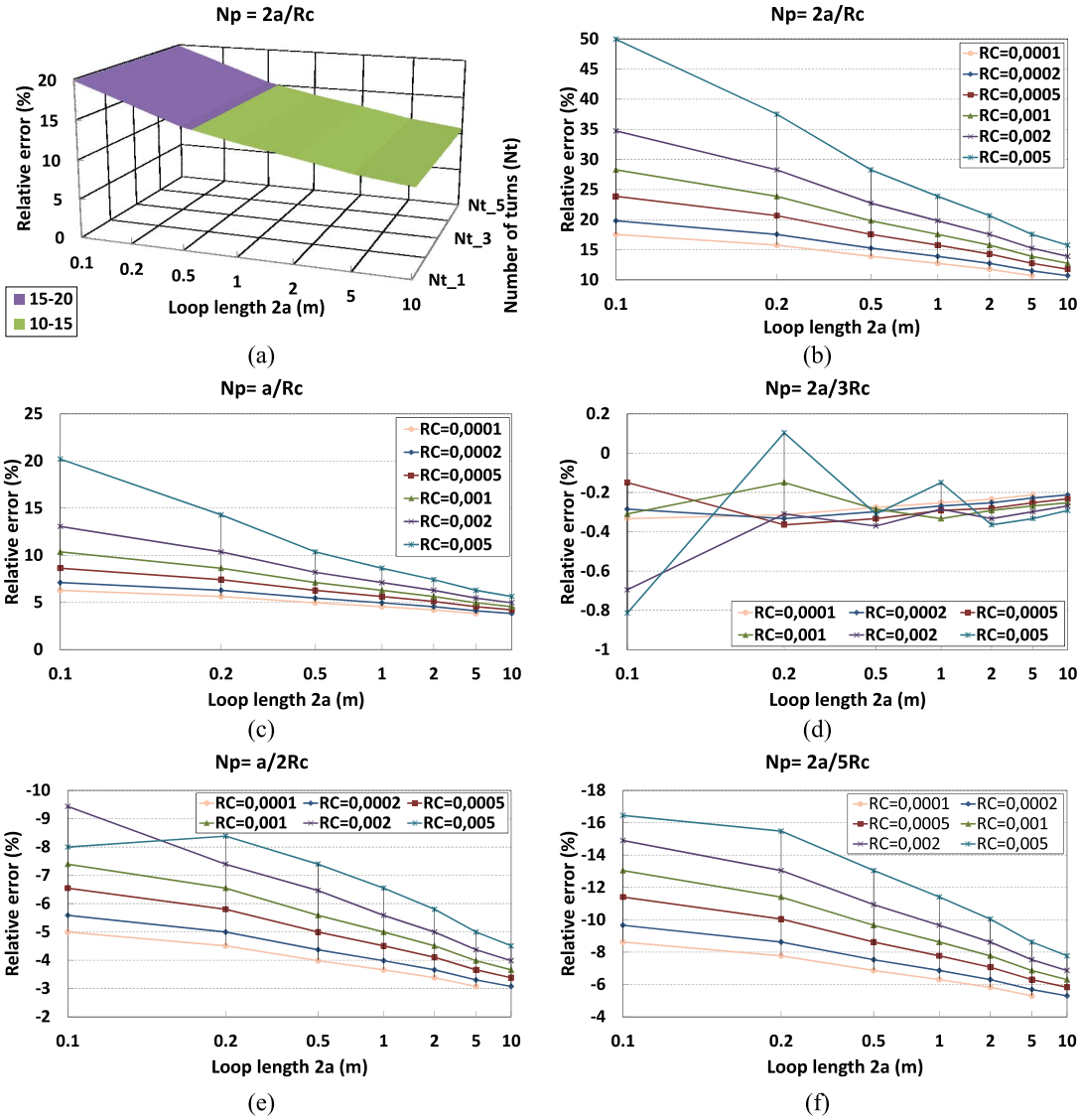

Fig. 3. Relative error between inductances calculated with (24) and (29) for different loop parameters and number of integration points Np. a) Np=2a/Rc for different turns and Rc=0.0002 m; b) Np=2a/Rc; c) Np=a/Rc; d) Np=2a/3Rc; e) Np=a/2Rc; f) Np=2a/5Rc.

Regarding the loop length, it has to be noticed that: a) for Intelligent Traffic Systems (ITS) applications loops dimensions are not smaller than 0.1 m, and b) for loop dimensions lower than 0.1 m the number of integration points given by (30) would decrease, the magnetic field fluctuations could not be properly followed and the difference with the theoretical calculations increased.

B. Second Order Effects

In previous studies it has not been considered that all the loop turns are not on the same coordinate z because of the conductors' dimensions. This effect was corrected by Mills [18], who derived new expressions for the inductance. In the case of N-turn equally separated rectangular loops, inductance is represented by:

$$L_{T,M} = NL_0 + 2\,(N-1)\,M_{12v} + 2\,(N-2)\,M_{13v} + \ldots \quad (31)$$

where L_0 is the self-inductance of a single turn rectangular loop, and M_{12v}, $M_{13v}\ldots$ are the mutual inductance between the loop turns.

L_0 is the sum of both internal, L_{0i}, and external, L_{0e}, inductance:

$$L_0 = L_{0i} + L_{0e} \quad (32)$$

L_{0i} is given by:

$$L_{0i} = 2\,(2a + 2b)L_i \quad (33)$$

Here, L_i is the inductance per unit length and, similarly as in (20), it must take into account the relationship between the inductance at a specific frequency and at low frequency (L_{i0}). This relationship was also given by Johnson [15] and is:

$$L_i = L_{i0}\frac{4}{q}\left[\frac{bei\,(q)\times bei'\,(q) + ber\,(q)\times ber'(q)}{(bei'\,(q))^2 + (ber'(q))^2}\right] \quad (34)$$

where the inductance at low frequency L_{i0} is given by:

$$L_{i0} = \frac{\mu_0\mu_r}{8\pi}(H/m) \quad (35)$$

Its value is $0.5\cdot10^{-7}$ H/m for copper conductors.

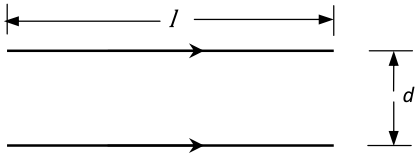

Fig. 4. Characteristics of two ideal, null cross section parallel conductors for mutual inductance measurement.

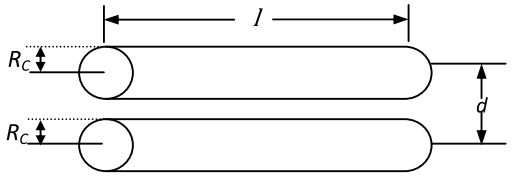

Fig. 5. Characteristics of two parallel conductors for mutual inductance measurement.

The calculation of L_{0e} can be derived from the concepts of mutual inductance, external self-inductance and from the method of mutual inductance. The mutual inductance of a pair of ideal parallel conductors, like the ones shown in Fig. 4, is derived in [19] and is given by:

$$M(l,d) = \pm\frac{\mu_0 l}{2\pi}\left\{ln\left[\frac{l}{d}+\sqrt{1+\left(\frac{l}{d}\right)^2}\right]+\frac{d}{l}-\sqrt{1+\left(\frac{d}{l}\right)^2}\right\} \tag{36}$$

In Fig. 4, l is the wires' length and d is the distance between them (both magnitudes in meters); the inductance will then be given in Henries. Equation (36) is positive when the current along both filaments has the same sense; otherwise it is negative.

The external self-inductance of a pair of conductors like the ones represented in Fig. 5 is given by:

$$L_P = L_1 - M_{12} + L_2 - M_{21}$$

where L_1 and L_2 are the self-inductance of the conductors whereas M_{12} and M_{21} are the mutual inductances measured from the conductors centers; it is assumed that the currents distribution is the same in the entire conductor's cross section. Self-inductances are of negative sign because the currents in conductors are of opposite sense. Since both conductors are of the same dimensions, one can write:

$$L = L_1 = L_2$$
$$M = M_{12} = M_{21}$$

Therefore:

$$L_P = 2(L - M)$$

In order to calculate the conductor external self-inductance the mutual inductance method is used [20]. In this method the conductor is replaced by two conductors of null cross section, separated by a distance equal to the conductor's radius. Therefore, the external self-inductance is given by:

$$L_P = 2(M(l, R_C) - M(l, d)) \tag{37}$$

From these results one can see that the external inductance L_{0e} of a one-turn rectangular loop is given by the sum of the inductance of two pairs of parallel conductors, L_{p1} and L_{p2}:

$$L_{0e} = L_{p1} + L_{p2}$$
$$L_{0e} = 2[M_1(l_1, R_C) - M_1(l_1, l_2) + M_2(l_2, R_C) - M_2(l_2, l_1)] \tag{38}$$

where $l_1 = 2a$ and $l_2 = 2b$.

As it can be concluded from (38), the external inductance of a one-turn rectangular loop equals the mutual inductance of two identical coaxial rectangular loops separated by the distance of the conductor's radius.

The mutual inductance of two parallel rectangular loops (like the ones shown in Fig. 6) can be obtained from the mutual inductances between parallel conductors.

In this way, the mutual inductance between two rectangular loops is given by:

$$M = -2\left[M_{13}\left(A, \sqrt{H^2+B^2}\right) - M_{11}(A, H) + M_{24}\left(B, \sqrt{H^2+A^2}\right) - M_{22}(B, H)\right] \tag{39}$$

In previous (39), terms M_{ij} are the mutual inductances between segment i of the lower loop and segment j of the upper loop. Factor 2 is because all the mutual inductances are symmetrical, and for every i and j, $M_{ij} = M_{ji}$.

Another formula to calculate the inductance was given by Niwa (1924) [21], and is:

$$\begin{aligned} L_N(\mu H) &= 0.008N^2\frac{aa_1}{b}\left[\frac{b}{2a_1}\sinh^{-1}\frac{a}{b}+\frac{b}{2a}\sinh^{-1}\frac{a_1}{b}\right. \\ &\quad -\frac{1}{2}\left(1-\frac{a_1^2}{b^2}\right)\frac{b}{a_1}\sinh^{-1}\frac{a}{b\sqrt{1+\frac{a_1^2}{b^2}}} \\ &\quad -\frac{1}{2}\left(1-\frac{a^2}{b^2}\right)\frac{b}{a}\sinh^{-1}\frac{a_1}{b\sqrt{1+\frac{a^2}{b^2}}} \\ &\quad -\frac{a_1}{2b}\sinh^{-1}\frac{a}{a_1}-\frac{a}{2b}\sinh^{-1}\frac{a_1}{a}+\frac{\pi}{2} \\ &\quad -\tan^{-1}\frac{aa_1}{b^2\sqrt{1+\frac{g^2}{b^2}}} \\ &\quad +\frac{b^2}{3aa_1}\sqrt{1+\frac{g^2}{b^2}}\left(1-\frac{g^2}{2b^2}\right) \\ &\quad +\frac{b^2}{3aa_1}-\frac{b^2}{3aa_1}\sqrt{1+\frac{a^2}{b^2}}\left(1-\frac{a^2}{2b^2}\right) \\ &\quad -\frac{b^2}{3aa_1}\sqrt{1+\frac{a_1^2}{b^2}}\left(1-\frac{a_1^2}{2b^2}\right) \\ &\quad \left.+\frac{b}{6aa_1}\left(\frac{g^3-a^3-a_1^3}{b^2}\right)\right] \end{aligned} \tag{40}$$

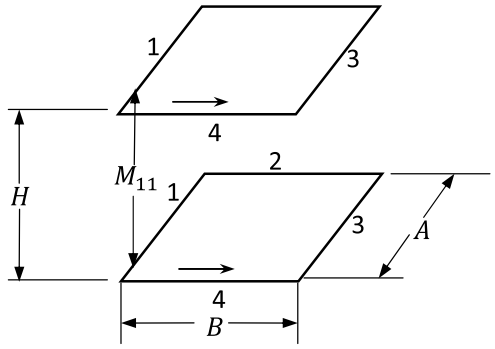

Fig. 6. Geometry for mutual inductance calculation between two coaxial parallel rectangular loops.

where:

- a :largest side of the loop
- a_1 :shortest side of the loop
- d $= 2R_C + 2E_a$: distance between two consecutive turns, where R_C is the conductor's radius and E_a is the insulator thickness
- b $= N{\cdot}d$: length of the loop
- g^2 $= a^2 + a_1^2$

Aside from the approximation presented from (24) to (28), two more approximations which refer to the inclusion in the integral calculation of the effect of cable's thickness follow. To this end, it is possible to correct the value of the flux crossing each turn of the loop by taking into account the separation between them. Then, in the case of an N-turn loop that carries a current of intensity I, the total inductance will be calculated using the fluxes $\emptyset_{K0}$ (magnetic flux generated by a certain turn on the plane were it is located), $\emptyset_{K1}$(flux generated by the turn adjacent to the one on which the flux is being measured), and $\emptyset_{Ki}$ (flux generated by the turn which is separated i turns from the one on which the flux is being measured). Consequently, the total inductance is given by:

$$L_{TI1} = \frac{N\emptyset_{K0} + 2\,(N-1)\,\emptyset_{K1} 2\,(N-2)\,\emptyset_{K2} + \cdots}{I} \tag{41}$$

where:

$$\emptyset_{K0} = \sum_{n=1}^{N_x-1} \sum_{m=1}^{N_y-1} B_K(-a+ndx, -b+mdy, 0) f_x f_y dy dx \tag{42}$$

Generally, for every $0 < i < N$, one can write:

$$\emptyset_{Ki} = \sum_{n=0}^{N_x} \sum_{m=0}^{N_y} B_K(-a+ndx, -b+mdy, idz) f'_x f'_y dy dx \tag{43}$$

In (43) dz is the separation between the conductors' centers of two consecutive turns. Besides, f'_x takes the value 1 in all points except when $n = 0$ or $n = N_x$, in which its value is 0.5. Similarly, f'_y takes the value 1 in all points except when $m = 0$ or $m = N_y$, in which its value is 0.5.

Another approximation to this case is obtained assuming that the total inductance is given by:

$$L_{TI2} = \frac{N\emptyset_{T2}}{I} \tag{44}$$

where the total equivalent flux $\emptyset_{T2}$ is approximated by the expression:

$$\emptyset_{T2} = \sum_{i=0}^{N-1} \sum_{n=0}^{N_x} \sum_{m=0}^{N_y} B_K(-a+ndx, -b+mdy, idz) f'_x f'_y dy dx$$

IV. Results With the Different Methods and Discussion

Below, the results about the calculation of the inductance generated by a rectangular loop which have been obtained with the different presented methods can be found.

Figure 7 shows the results obtained for different loop dimensions, number of turns and the different models (methods) that have been developed in this work. Conductor's radius and insulator's width are supposed constant, their values being 0.001 m and 0.0005 m, respectively. These results correspond only to squared loops where $2a = 2b$. The assumption made for all cases is that oscillation frequency is 20 kHz, current intensity is 100 mA, the width of the cavity where the loops are placed is 4.5 mm and tan δ of pavement is 0.01. All these values are usually found in the loops used for vehicles detection. Besides, only 40 terms of the Bessel functions have been used, and the number of points taken for the numeric integration is:

$$N_x = N_y = \frac{2a}{3R_C} = \frac{2b}{3R_C}$$

In Fig. 7e) and 7f) the length of each side are 1 m and 2 m respectively.

Previous results demonstrate that integral calculation methods are appropriate to calculate the self-inductance (L_{TI1}, L_{TI2} and L_ϕ). In this sense, it is worth highlighting the strong similarity between the results obtained with the three alternative methods of numeric calculation and the three usual standard models. So, one can remark the strong resemblance between L_ϕ and $L_{f,G}$, between L_{TI1} and L_N and ultimately, between L_{TI2} and $L_{T,M}$. Therefore, this can validate the adoption of a similar method to obtain the mutual inductance between two rectangular loops. This mutual inductance appears between the buried loop and the one which represents the vehicle's contour.

A. Theoretical Model Verification

In order to confirm the calculations correctness several loops were built and the magnetic fields generated by them were measured [22]. The measured values were then compared with theoretical ones obtained from (17). The characteristics of one of the used loops were the following.

- Type of conductor: finned copper connecting cable, polyvinyl chloride coated, and cross section 0.28 mm^2. Mills Equations were used with Rc = 0.0002985 and insulator width of 0.0002.

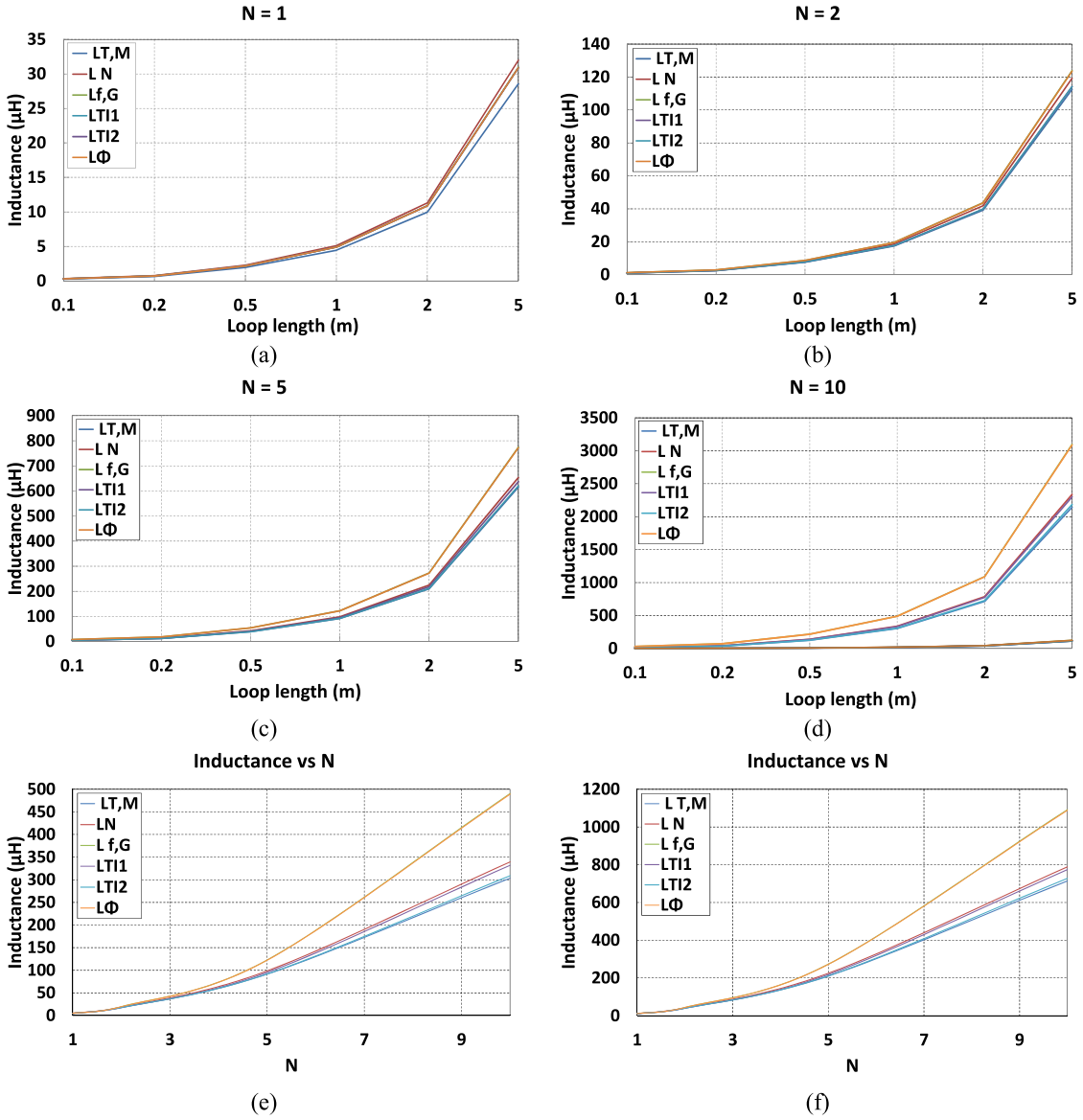

Fig. 7. Inductance values obtained in different ways. In the sub-figures from a) to d) inductance is given for different loop lengths, the parameters being the different used methods or models and the number of turns Nt. In sub-figures e) and f) inductance is calculated for the different number of turns, the parameter being the different used models. Sub-figure e) is obtained for a loop of 1m for each side whereas in f) is obtained for a loop of 2 m per side.

- Number of turns: 5
- Dimensions: 1.30x0.80 m

Using these characteristics, the inductance was obtained by means of two methods. On the one hand, it was measured with an LCR meter, manufactured by PROMA, type MZ-505, at 1 kHZ, and the following values were obtained:

- L = 112.1 μH (Q = 0-512), C = 46.22 μF, R = 1.75 Ω

On the other hand, the same parameters where obtained from Mills Equations, thus yielding:

- L=113.25 μH (Q=0.548), C=223.66 μF, R=1.298Ω at 1kHz.

The magnetic field was generated with a 37.76 mA rms sinusoidal current at a frequency of 139.7 kHz. It was measured with the magnetic field meter Exposure Level Tester ELT-400. The sensor of this device has a spherical shape with a diameter of 12.5 cm and contains loops by which the magnetic field is detected.

The magnetic field generated in this way was measured by placing the ELT-400 meter on a 2 cm height basis. Thereafter, the device was horizontally displaced along the main central axis of the loop. Readings were undertaken every 2 cm. $|\vec{B}|$ calculations were performed for a height of 8.25 cm, which corresponds to the sum of the platform above which the ELT-400 was placed, plus 6.25 cm of the sensor radius.

In Fig.8, one can see the superposition of both the measured and the calculated values obtained with the herein developed Equations.

The mismatch observed in Fig. 8 around the peaks between experimental data and theoretical calculations are due to the singularity presented by the electric field Equation on the conductor. In the proximity of the conductor, the electric field variations are very strong and therefore a small deviation in the measuring point yields highly noticeable changes in readings. Besides, the measuring instrument sensor has a diameter of 12.5 cm and the given measured value is the integral of

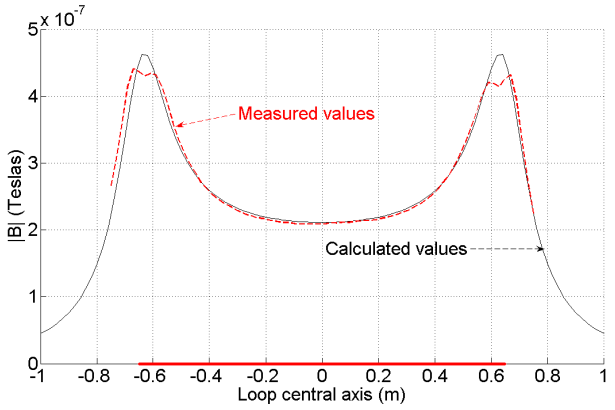

Fig. 8. Comparison between measured and calculated values of the magnetic field.

the electric field in the surface where the measurement is performed.

B. Discussion

The key idea of this study is that the proposed numerical method provides results which are comparable with those obtained with classical methods. Nevertheless, whereas the latter are only applicable to a specific geometry, our method can be used to the study of any geometry.

Moreover, classical methods provide the inductance value of a rectangular loop, but they do not allow the visualization of the generated magnetic field and how it interacts with other structures (the vehicles passing over them), thus determining a modification of the global inductance. However, our method makes it possible, as will be shown in our next works.

V. Conclusions

In this work, a comparison between the magnetic field values obtained in different ways has been performed. To this end, different Equations that allow the magnetic field calculation have been presented and the results have been compared with those generated by means of a method of numeric integration. This method uses a specific size for the integration intervals (cells). The obtained expressions are of general character, the only restrictions being a small conductor cross section and stationary currents. This allows the magnetic field calculation at distances of the some order of magnitude than the loop dimensions, which in turn are the distances of interest in applications like the precise detection of metallic elements or short distance communications by means of magnetic inductance.

Comparisons of both magnetic field real measurements and theoretical results were performed thus verifying the goodness of model results. These results show that the obtained Equations yield a good enough approximation to real values, and therefore they can be a tool for the design of rectangular loops.

Although the hereinabove described formulas correspond to a rectangular loop, the same procedure might apply to any type of loop formed by rectilinear segments located on a plane.

The obtained results might help considerably to analyze some phenomena like:

- The error that can be made when estimating a vehicle size if one takes only into account the moments of activation and deactivation of the electronic units which control the loop sensors.
- The magnetic imprint most appropriate amplitudes band that must be used to estimate the vehicles speed by means of only one loop.
- The coverage area of a short range wireless communication system between vehicles and infrastructures by means of magnetic coupling.

All this involves the need for analyzing each loop response. If the presented model is appropriate all these analyses will be carried out by means of very simple electric measurements and simulation technics.

In the next works, the results obtained in these fields will be presented.

References

[1] E. B. Hoekman and S. M. Hamer, "Vehicle detector with series resonant oscillator drive," U.S. Patent 5 153 525 A, Oct. 6, 1992.

[2] L. A. Klein, D. R. P. Gibson, and M. K. Mills, "Traffic detector," Lawrence A Klein, FHWA-HRT-06-108, 3rd ed., vol. 1. Oct. 2006. [Online]. Available: http://www.fhwa.dot.gov/publications/research/operations/its/06108/06108.pdf

[3] R. L. Anderson, "Electromagnetic loop vehicle detectors," *IEEE Trans. Veh. Technol.*, vol. 19, no. 1, pp. 23–30, Feb. 1970.

[4] A. Arroyo-Núñez and A. Mocholí-Salcedo, "Sistemas sensores empleados en ITS," in *Proc. 7th Congr. Español Sistemas Intell. Transp.*, Valencia, Spain, Sep. 2007.

[5] S. G. Burns. (2009). *In-situ* vehicle classification using an ILD and a magnetoresistive sensor array. Intelligent Transportation Systems, Institute Center for Transportation Studies, University of Minnesota, Minneapolis, MN, USA. [Online]. Available: http://www.its.umn.edu/Publications/ResearchReports/reportdetail.html?id=1750

[6] J. H. Arroyo-Núñez, A. Mocholí-Salcedo, R. Barrales-Guadarrama, and A. Arroyo-Nuñez, "Communication between magnetic loops," in *Proc. 16th World Road Meeting*, Lisbon, Portugal, May 2010.

[7] B. R. Hellinga, "Improving freeway speed estimates from single-loop detectors," *J. Transp. Eng.*, vol. 128, pp. 58–67, Jan./Feb. 2002.

[8] A. Tok, S. V. Hernandez, and S. G. Ritchie, "Accurate individual vehicle speeds from single inductive loop signatures," in *Proc. 88th Annu. Meeting Transp. Res. Board*, 2009, paper #09-3512.

[9] M. L. Hazelton, "Estimating vehicle speed from traffic count and occupancy data," *J. Data Sci.*, vol. 2, no. 3, pp. 231–244, 2004.

[10] S. R. Hilliard, "Vehicle speed estimation using inductive vehicle detection systems," U.S. Patent 6 999 886 B2, Feb. 14, 2006.

[11] M. K. Mills, "Self inductance formulas for quadrupole loops used with vehicle detectors," in *Proc. 35th IEEE Veh. Technol. Conf.*, May 1985, pp. 81–87.

[12] C. T. A. Johnk, *Teoría Electromagnética: Campos y ondas*. Limusa-Noriega, Ed. México, 1999.

[13] M. Misakian, "Equations for the magnetic field produced by one or more rectangular loops of wire in the same plane," *J. Res. Nat. Inst. Standards Technol.*, vol. 105, no. 4, p. 557, Jul./Aug. 2000. [Online]. Available: http://www.nist.gov/jres

[14] R. M. Spiegel and J. L. Lorenzo-Avellanas, *Fórmulas y Tablas de Matemática Aplicada*. New York, NY, USA: McGraw-Hill, 1999, p. 226.

[15] W. C. Johnson, *Transmission Lines and Networks*. New York, NY, USA: McGraw-Hill, 1950.

[16] M. K. Mills, "Inductive loop system equivalent circuit model," in *Proc. IEEE 39th Veh. Technol. Conf.*, vol. 2. May 1989, pp. 689–700.

[17] F. W. Grover, *Inductance Calculations: Working Formulas and Tables*. New York, NY, USA: Dover, 1962, p. 34.

[18] M. K. Mills, "Self inductance formulas for multi-turn rectangular loops used with vehicle detectors," in *Proc. 33rd IEEE Veh. Technol. Conf.*, vol. 33. May 1983, pp. 65–73.

[19] S. Seely, *Introduction to Electromagnetic Fields*. New York, NY, USA: McGraw-Hill, 1958, pp. 185–186.

[20] S. Ramo, J. R. Whinnery, and T. van Duzer, *Fields and Waves in Communication Electronics*. Hoboken, NJ, USA: Wiley, 1965, pp. 309–311.

[21] Y. Niwa, *A Study of Coils Wound on Rectangular Frames With Special Reference to the Calculation of Inductance*, vol. 141. Tokyo, Japan: Researches of the Electro-technical Laboratory, Apr. 1924.

[22] J. H. A. Núñez, "Estudio del comportamiento magnético de espiras rectangulares para la transmisión de información de corto alcance en sistemas inteligentes de transporte," Ph.D. dissertation, Dept. Elect. Eng., Polytech. Univ. Valencia, Valencia, Spain, 2016.

Antonio Mocholí-Salcedo received the Ph.D. degree in industrial engineering from Universitat Politècnica de València, Spain, in 1991.

He is a Professor with the Department of Electronic Engineering, Universitat Politècnica de València, where he is also the Coordinator with the Traffic Control Systems Group, ITACA Institute.

José Humberto Arroyo-Núñez received the M.Sc. degree in 2002 from the National Institute of Astrophysics, Optics and Electronics, México, and the Ph.D. degree in electronic engineering from Universitat Politècnica de València, Spain, in 2016.

He is an Assistant Professor with the Department of Electronic and Telecommunications Engineering, Polytechnic University of Tulancingo, Mexico, where he is also a Co-Ordinator.

Víctor M. Milián-Sánchez received the Ph.D. degree in Physics from Universitat Politècnica de València, Spain, in 2014.

He is an Invited Researcher with the Chemical and Nuclear Engineering Department, Institute of Industrial, Radiological and Environmental Safety, Universitat Politècnica de València, Spain.

María J. Palomo-Anaya received the B.S. degree in industrial engineering from Universitat Politècnica de València, Spain, in 1998, where she is currently working toward the Ph.D. degree.

She was an Assistant Professor with Universitat Politècnica de València. Her research interest and works are in the area of signal analysis.

Alexander Arroyo-Núñez received the M.Sc. degree in electronic engineering from Polytechnic University of Valencia, Spain, in 2002, where he is currently working toward the Ph.D. degree with the Department of Electronic Engineering.

He is the Director of the Academic Program of Biomedical Engineering with the Polytechnic University of Chiapas, Mexico.